First published in:
FUNCTIONAL MATERIALS

FULL PAPER

DOI: 10.1002/adfm.200601074

Fabrication of Silicon Inverse Woodpile Photonic Crystals**

By *Martin Hermatschweiler*,* *Alexandra Ledermann*, *Geoffrey A. Ozin*, *Martin Wegener*, and *Georg von Freymann**

Silicon inverse woodpile photonic crystals are fabricated for the first time. Our approach, which is based on direct laser writing of polymeric templates and a novel silicon single-inversion procedure, leads to high-quality structures with gap/midgap ratios of 14.2 %, centered at a wavelength of 2.5 μm. It is shown that gap/midgap ratios as large as 20.5 %, centered at 1.55 μm, may become possible in the future.

1. Introduction

Shortly after the introduction of the concept of photonic bandgap materials by John and Yablonovitch in 1987,[1,2] Ho, Chan, and Soukoulis[3] reported in 1990 that certain structures with a diamondlike symmetry can exhibit complete 3D photonic bandgaps (PBG). A prominent example of such a "semiconductor for light" is the so-called woodpile or logpile structure. This structure reveals an 18 % gap/midgap ratio when fabricated out of silicon with a volume filling fraction (*f*) of 30 %.[4] The inverse woodpile structure shows an even larger gap: For slightly ellipsoidal air rods (aspect ratio 5:4) a gap/midgap ratio of 28 % has been predicted theoretically for a silicon volume filling fraction of 18 %.[4] This record still stands.

Thus far, however, it has not been possible to actually fabricate *inverse* silicon woodpiles by any means in any frequency range. Here, we realize this important structure by using direct laser writing of polymeric templates and subsequently a silicon single-inversion (SSI) procedure—which is described here for the first time.

In 2006, we introduced the silicon double-inversion (SDI) procedure:[5] First, polymer templates were fabricated by direct laser writing (DLW)[6–11] or other means. Unfortunately, these polymeric templates (SU-8, MicroChem Corp.) alone did not withstand the temperatures required for infiltration with Si via chemical vapor deposition (CVD). Thus, we introduced an intermediate step, that is, inversion with silica via an atomic layer deposition (ALD) process at room temperature.[12] Next, the polymer was removed and silicon was deposited[13] in the silica inverse structure. Finally, the silica was etched out, leading to a high-quality silicon *positive* replica of the original polymer structure.[5] Related approaches have also been published by other groups.[14,15]

Herein, we modify the SDI process to SSI: Rather than completely filling the polymer template with silica, we only provided a thin silica coating. Subsequently—without removing the polymer—we infiltrated the composite structure with silicon via silicon CVD. Amazingly, the thin silica coating provided sufficient and reliable stabilization for the high-temperature silicon CVD process, in which the polymer melted but retained its shape because of the silica coating. Furthermore, the polymer could not be calcined owing to the lack of oxygen. Finally, the silica was etched out and the polymer was calcined in air, leading to a silicon *inverse* of the previously silica-coated polymeric template. Incidentally, the intermediate silica-coating step very favorably reduced the aspect ratio of the elliptical woodpile rods made by DLW as well as the silicon volume filling fraction of the final Si inverse woodpile structure.

2. Results and Discussion

We started with the fabrication of SU-8 woodpile templates: The main DLW process parameters were similar to those we have reported earlier.[8,9,11] In addition, we introduced a shaded-ring filter (SRF)[16–19] into the optical path (directly in

[*] M. Hermatschweiler, Dr. G. von Freymann, Prof. M. Wegener
Institut für Angewandte Physik, Universität Karlsruhe (TH)
76128 Karlsruhe (Germany)
E-mail: martin.hermatschweiler@physik.uni-karlsruhe.de; freymann@int.fzk.de
M. Hermatschweiler, Dr. G. von Freymann, Prof. M. Wegener
DFG-Center for Functional Nanostructures (CFN)
Universität Karlsruhe (TH)
76128 Karlsruhe (Germany)
Dr. G. von Freymann, A. Ledermann
Institut für Nanotechnologie
Forschungszentrum Karlsruhe in der Helmholtz-Gemeinschaft
76021 Karlsruhe (Germany)
Prof. G. A. Ozin
Materials Chemistry Research Group
Department of Chemistry, University of Toronto
80 St. George Street, Toronto, ON M5S 3H6 (Canada)

[**] We acknowledge support provided by the Deutsche Forschungsgemeinschaft (DFG) and the State of Baden-Württemberg through the DFG-Center for Functional Nanostructures (CFN) within subproject A1.4. The research of G.v.F. is further supported through a DFG Emmy-Noether fellowship (DFG-Fr 1671/4-3). G.A.O. is Government of Canada Research Chair in Materials Chemistry. He is indebted to the Natural Sciences and Engineering Research Council of Canada for support of this research and the CFN for a Guest Professorship.

front of the microscope objective lens) to specifically design the intensity distribution in the focal region. Without a SRF, the aspect ratio of the elliptical rods comprising the SU-8 woodpile was ca. 2.7, which was limited by the numerical aperture $NA = 1.4$ of the oil-immersion lens. This ratio of 2.7 is much larger than the desired ratio of 5:4 for an optimum inverse woodpile structure. By inserting the SRF the axial elongation of the rods could be reduced to a value of about 2, which is very favorable for the magnitude of the PBG of the final silicon inverse woodpile.

The atmospheric pressure, room temperature silica ALD process consisted of a sequential saturation of the template surfaces with water and reaction with $SiCl_4$ (N_2 was used as carrier gas) to deposit amorphous SiO_2 in a layer-by-layer fashion, while releasing the silica condensation-polymerization catalyst HCl. The thickness deposited in each cycle could be tuned in the range of several tens of nanometers per cycle. Clearly, coating of an elliptical rod from all sides reduces its aspect ratio as the layer thickness increases. Coating an SU-8 rod with a lateral diameter of 220 nm with 205 nm of silica reduces the aspect ratio from 2 to 1.35. Thicker coatings further reduce the aspect ratio, but lead to an unfavorable air volume fraction (which finally determines the silicon filling fraction). As an example, such a silica-coated SU-8 woodpile structure is schematically depicted in Figure 1a.

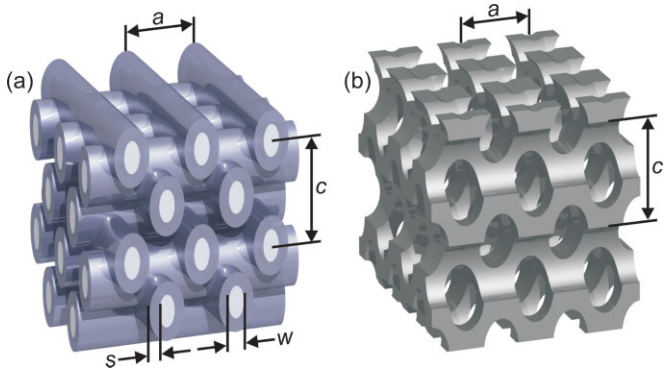

Figure 1. Schematic illustration of the SSI method for the familiar woodpile structure with in-plane rod-distance *a* and lattice constant *c* along the stacking direction. a) The rods of initial lateral diameter *w* are coated with silica of thickness *s*. b) The structure of (a) after inversion with silicon.

Next, the SU-8/silica composite structure was infiltrated by Si low-pressure CVD using disilane (Si_2H_6) as precursor (parameters are detailed in the Experimental section). The deposition process was stopped when the pores were completely infiltrated, at which point the Si covered the entire structure as well as the glass substrate.

At this point, reactive ion etching (RIE) with Ar-diluted SF_6 was applied to remove the Si cap layer that would otherwise inhibit the removal of the polymer as well as the silica. Subsequent wet-etching of the silica and calcination of the polymer resulted in a Si single-inverted woodpile (Fig. 1b), completely processed on one glass substrate. Keeping the same substrate—in contrast to the work we reported earlier[5]—during all process steps is of major importance: Now, the Si photonic crystal is free-standing and no longer embedded in an optical adhesive. This could provide the possibility for in-plane optical characterization of 3D Si photonic crystals. For example, Si replicas/inverse structures of 3D–2D–3D photonic crystal heterostructure templates with incorporated waveguides[20] are now within reach. Altogether, the fabrication and conversion of high-quality polymer templates into Si inverse structures by means of SSI can routinely be performed within 1.5 days.

Figure 2 shows a typical focused-ion-beam (FIB) cut of the resulting silicon inverse woodpile structure. Parameters are $a = 0.977$ μm, $c = 1.125$ μm (i.e., a sample compressed relative to the face-centered cubic (fcc) translational symmetry), rod aspect ratio $\chi = 1.78$, and Si volume filling fraction $f = 35.8\,\%$.

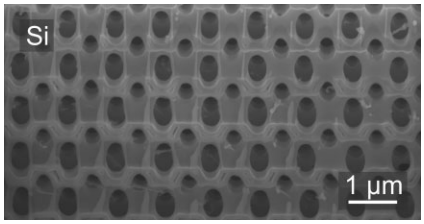

Figure 2. Electron microscopy image of a Si inverse woodpile, cut by a focused ion beam (FIB) to reveal the internal structure and quality.

Obviously, the achieved *structural* quality is very high. The small grains in Figure 2 result from the FIB cuts. To verify that the SU-8 neither combusted nor vaporized during the Si CVD, we fabricated a sample with parameters identical to those of Figure 2, applied the same amount of silica by ALD, and subjected the sample to the Si CVD process. Despite heating the sample to the deposition temperature under high vacuum—removing the flow of disilane and keeping the temperature for 1 h—the SU-8 was not damaged, and was clearly protected by the silica coating (Fig. 3).

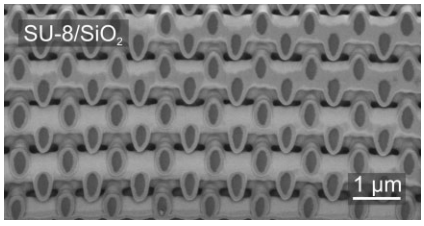

Figure 3. As Fig. 2, but for the SU-8/silica composite structure (i.e., the disilane flow was not applied in the Si CVD). The SU-8 (dark gray) is enclosed by a thin layer of silica (bright gray).

To assess the *optical* quality of our structures after each process step, we performed optical transmittance and reflectance experiments (Fig. 4). The instrument used for this purpose was a commercial microscope Fourier-transform spectrometer that has been described in detail previously.[8,9] For reference, we

ADVANCED FUNCTIONAL MATERIALS

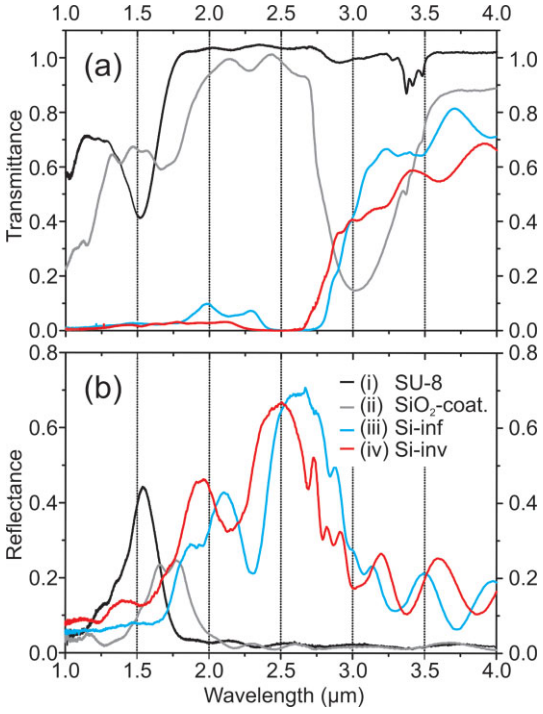

Figure 4. Optical transmittance (a) and reflectance (b) spectra of one woodpile sample in different stages of the process (i)–(iv).

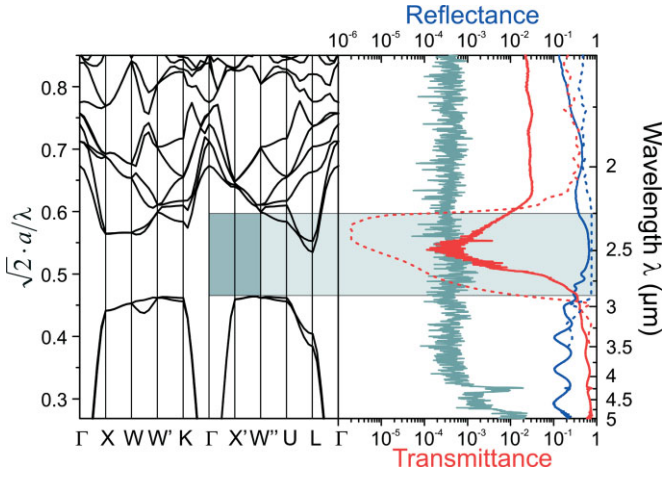

Figure 5. Calculated band structure (left) of a sample with parameters taken from an FIB cut. A complete 3D PBG with a gap/midgap ratio of 14.2 % can be seen. On the right, scattering-matrix calculations (dashed curves) are compared to measurements (solid curves). The minimum transmittance is instrument-limited, as can be seen by comparison of transmittance measurements from an opaque sample (gray noise, right).

used the bare glass substrate and a silver mirror, respectively. Figure 4a and b shows measured transmittance and reflectance spectra, respectively, of a sample similar to that depicted in Figures 2 and 3. In the beginning, a pronounced stop band is visible for the SU-8 woodpile at ca. 1.5 μm (i), which shifts red and gets weaker after coating the polymer with silica because of an increase of the average refractive index (ii). The striking transmittance dip at a wavelength of ca. 3 μm originates from absorption of water by the silica. After infiltration with Si (iii) and removal of the polymer and silica, a pronounced transmittance dip at a wavelength of ca. 2.5 μm is observed with a minimum transmittance value of less than 10^{-3}, which becomes visible when the data are plotted on a logarithmical scale (see solid red line in Fig. 5, right-hand side (rhs)). This value is instrument-limited, as confirmed by independent control experiments on thick anodized metal plates (see gray noisy curve in Fig. 5, rhs). The structural parameters of the resulting Si inverse woodpile are as follows: $a = 0.95$ μm, $c = 1.344$ μm (i.e., a sample with fcc translational symmetry), $\chi = 1.47$, and $f = 33.5\,\%$.

To allow for comparison with theory, we performed bandstructure[21] and scattering-matrix calculations[22] for the structural parameters given above. Note that any deposition of solids from the gas phase leaves behind small air voids in 3D structures as soon as bottlenecks close (see Fig. 2). This effect clearly reduces the effective refractive index n_{eff}. To calculate this value, the effective Si volume filling fraction was taken as $f_{\mathrm{eff}} = 77.2\,\%$ in order to fit the measured optical spectra. This filling fraction is consistent with Figure 2. In the spirit of an effective material, we use $n_{\mathrm{eff}} = 3.95 \times f_{\mathrm{eff}} + 1 \times (1 - f_{\mathrm{eff}})$. The value of 3.95 corresponds to the measured refractive index of a thin film of amorphous Si. This finally leads to $n_{\mathrm{eff}} = 3.28$. The resulting band structure, shown on the left-hand side of Figure 5, is consistent with our optical experiments along the $\Gamma X'$ direction and reveals a complete 3D PBG with a gap/midgap ratio of 14.2 %. To compare the band structure with experimental results we also had to take the $\Gamma W''$-direction into account. In addition, we performed scattering-matrix calculations for a sample consisting of 20 layers. The spectra were calculated accounting for the finite opening angle in the experiment: We averaged the reflectance and transmittance data achieved for plane waves impinging onto the samples from different orientations, taking into account angles of incidence between 15° and 30°. This mimics the experimental setup, where a Cassegrain objective was used for focusing light onto the sample. Clearly, the position of the stop band (see gray area in Fig. 5) must not be confused with that of the PBG. The observed and calculated stop bands agree qualitatively. Deviations are likely to be the result of sample imperfections and/or the simplicity of our modeling. Specifically, the measured transmittance on the short-wavelength side of the stop band is lower than the calculated one. This could be due to variations in the size of the small air voids that can be seen in the FIB cut in Figure 2 and/or the remaining surface roughness.

Finally, we evaluated how much future improvement would still be possible under realistic assumptions. This brings us to the gap map depicted in Figure 6. Here, the width of the PBG after SSI is depicted as a function of the initial lateral diameter of the SU-8 rods (w) and the thickness (s) of the silica coating deposited on the polymer surfaces, both relative to the in-plane distance a of neighboring rods of the woodpile. Again, a reduced effective refractive index of 3.28 is assumed for an fcc translational symmetry ($(c/a)^2 = 2$). To take into account the ex-

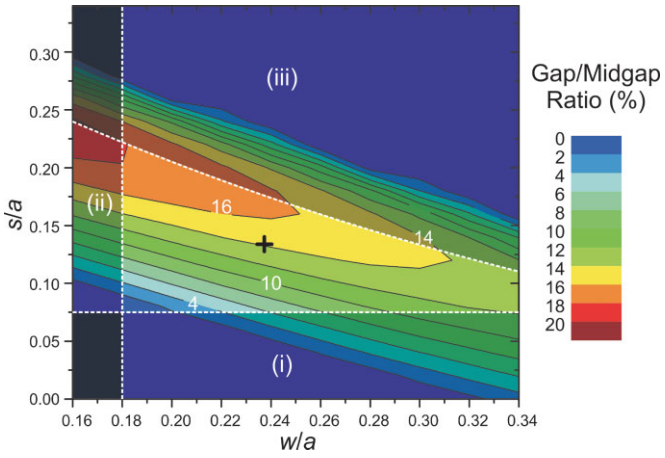

Figure 6. Gap map of Si inverse woodpile structures with fcc translational symmetry (i.e., $c = 2^{1/2}a$) The gap/midgap ratio is plotted vs. the initial lateral width of the SU-8 rods w and the silica thickness s deposited on all surfaces, both relative to the in-plane rod distance a. Experimentally inaccessible areas are grayed out (see (i)–(iii) and main text).

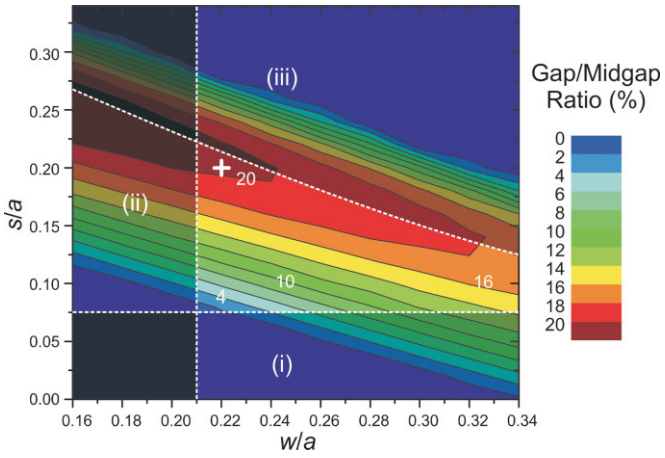

Figure 7. Same as Figure 6, but for structures with lattice constant $c = 1.15 \times 2^{1/2}\,a$. Notably, gap/midgap ratios of up to 20.5 % are within reach (marked with a white cross).

perimentally accessible range, we grayed out three areas for the following reasons: i) To prevent the polymer from losing its shape during the Si CVD process, a minimum amount of silica needs to be deposited. ii) The template itself must meet the condition that the rods are connected. iii) For the sake of the optical quality of the Si photonic crystal, we also grayed out areas where the hollowness of the Si structure would no longer justify the assumption of a homogeneous Si with an effective refractive index, although the sample may still be mechanically stable. Under these assumptions, a broad range of parameters for which high-quality inverse Si woodpiles can be fabricated still remains, with gap/midgap ratios of the PBG of up to 18 %. The optically characterized sample (see Fig. 5) is marked in Figure 6 with a black cross.

Finally, we optimized the woodpile design by increasing the lattice constant c by 15 % along the stacking direction relative to fcc translational symmetry. The resulting gap map in Figure 7 is plotted in a similar manner as Figure 6. Notably, gap/midgap ratios of up to 20.5 % are within reach (marked with a white cross). To bring the gap center position to 1.55 μm wavelength, a rod distance of $a = 600$ nm would be necessary.

3. Conclusions

We fabricated and characterized the first silicon inverse woodpile photonic crystals. Electron microscopy images and optical spectroscopy compared with band structure calculations revealed high sample quality. We have argued that the achieved gap/midgap ratio of 14.2 % can further be increased up to 20.5 % with the presented silicon-single-inversion process. Furthermore, the PBG can likely be shifted to telecommunication wavelengths in the near future by improvements in direct laser writing of polymeric templates.

4. Experimental

For a detailed description of the fabrication of the polymer templates *via* direct laser writing, we refer to our previous publications [8,9,11].

Room Temperature, Atmospheric Pressure Silica ALD: First, after an initial flushing of the deposition chamber with N_2 for more than 30 min, the N_2 flow of 300 sccm was directed through a bubbler filled with double-distilled H_2O for 5 min, leading to a physisorbed water layer on the sample surfaces. Subsequently, the chamber was flushed with N_2 for 5 min. The N_2 flow was then directed for 1.5 min through a bubbler containing $SiCl_4$ (Sigma–Aldrich 13 736, > 99 %), which led to growth of approximately 30–40 nm of dense, amorphous SiO_2 (silica) per cycle on the sample surfaces while releasing HCl. This sequence was repeated until the woodpile was coated with the desired thickness.

Silicon CVD: For the Si CVD, the silica-coated woodpile was slowly ($t > 2$ h) heated to the deposition temperature of 470 °C. We used disilane (Si_2H_6) (Linde disilane 4.8) as a precursor. For the deposition, a disilane flow of 1 sccm at 5.0 mbar was maintained for 1 h, which led to a deposition rate of approximately 6 nm min^{-1}.

Reactive-Ion Etching (RIE): The Si cap layer was removed by RIE in an SF_6-Ar plasma (10 sccm SF_6, 30 sccm Ar) at a pressure of 22 mTorr (1 Torr ≈ 133.3 Pa) and 70 W forward power (Oxford Plasmalab 80 Plus RIE system). The etch rate was about 125 nm min^{-1}.

Removal of Silica: A few drops of 1 vol % aqueous HF were placed on the sample. After 15 min the sample was rinsed with distilled water and dried in a soft flow of nitrogen. The procedure was repeated twice until no more silica was left.

Removal of SU-8: SU-8 was removed either by RIE with an O_2 plasma (same system as above) or via calcination in air at 430 °C ($t > 6$ h, tube furnace Carbolite MTF 12/38/400).

Optical Characterization: Measurements on the woodpile were taken by using a near-IR Fourier transform spectrometer (Bruker Equinox 55, NIR halogen source) connected to a microscope (Bruker Hyperion 1000, 36× Cassegrain lens, numerical aperture 0.5, liquid N_2-cooled InSb detector).

For the numerical calculations we used the freely available MIT photonic bands package [21] (band structure) and our own scattering matrix code based on the literature [22].

Received: November 8, 2006
Revised: February 19, 2007
Published online: August 17, 2007

ADVANCED FUNCTIONAL MATERIALS

Note added in proof: An method analogous to the fabrication process describe here has simultaneously been developed for the fabrication of germanium inverse woodpile structures [23].

[1] S. John, *Phys. Rev. Lett.* **1987**, *58*, 2486.
[2] E. Yablonovitch, *Phys. Rev. Lett.* **1987**, *58*, 2059.
[3] K. M. Ho, C. T. Chan, C. M. Soukoulis, *Phys. Rev. Lett.* **1990**, *65*, 3152.
[4] K. M. Ho, C. T. Chan, C. M. Soukoulis, R. Biswas, M. Sigalas, *Solid State Commun.* **1994**, *89*, 413.
[5] N. Tétreault, G. von Freymann, M. Deubel, M. Hermatschweiler, F. Pérez-Willard, S. John, M. Wegener, G. A. Ozin, *Adv. Mater.* **2006**, *18*, 457.
[6] H. B. Sun, S. Matsuo, H. Misawa, *Appl. Phys. Lett.* **1999**, *74*, 786.
[7] S. Kawata, H. B. Sun, T. Tanaka, K. Takada, *Nature* **2001**, *412*, 697.
[8] M. Deubel, G. von Freymann, M. Wegener, S. Pereira, K. Busch, C. M. Soukoulis, *Nat. Mater.* **2004**, *3*, 444.
[9] M. Deubel, M. Wegener, A. Kaso, S. John, *Appl. Phys. Lett.* **2004**, *85*, 1895.
[10] K. K. Seet, V. Mizeikis, S. Matsuo, S. Juodkazis, H. Misawa, *Adv. Mater.* **2005**, *17*, 541.
[11] M. Deubel, M. Wegener, S. Linden, G. von Freymann, *Appl. Phys. Lett.* **2005**, *87*, 221 104.
[12] H. Míguez, N. Tétreault, B. Hatton, S. M. Yang, D. Perovic, G. A. Ozin, *Chem. Commun.* **2002**, 2736.
[13] A. Blanco, E. Chomski, S. Grabtchak, M. Ibisate, S. John, S. W. Leonard, C. Lopez, F. Meseguer, H. Míguez, J. P. Mondia, G. A. Ozin, O. Toader, H. M. van Driel, *Nature* **2000**, *405*, 437.
[14] A. Blanco, C. López, *Adv. Mater.* **2006**, *18*, 1593.
[15] G. M. Gratson, F. García-Santamaría, V. Lousse, M. Xu, S. Fan, J. A. Lewis, P. V. Braun, *Adv. Mater.* **2006**, *18*, 461.
[16] C. Ibáñez-López, G. Saavedra, G. Boyer, M. Martínez-Corral, *Opt. Express* **2005**, *13*, 6168.
[17] M. Martínez-Corral, C. Ibáñez-López, G. Saavedra, M. T. Caballero, *Opt. Express* **2003**, *11*, 1740.
[18] P. Török, P. Varga, *Appl. Opt.* **1997**, *36*, 2305.
[19] P. Török, P. Varga, G. R. Booker, *J. Opt. Soc. Am. A* **1995**, *12*, 2136.
[20] M. Deubel, M. Wegener, S. Linden, G. von Freymann, S. John, *Opt. Lett.* **2006**, *31*, 805.
[21] S. G. Johnson, J. D. Joannopoulos, *Opt. Express* **2001**, *8*, 173.
[22] D. M. Whittaker, I. S. Culshaw, *Phys. Rev. B* **1999**, *60*, 2610.
[23] F. García-Santamaría, M. Xu, V. Lousse, S. Fan, P. V. Braun, J. A. Lewis, *Adv. Mater.* **2007**, *19*, 1567.